

Time delay and magnification centroid due to gravitational lensing by black holes and naked singularities

K. S. Virbhadra*

Department of Mathematics, Physics and Statistics, University of the Sciences in Philadelphia,
Philadelphia, Pennsylvania 19104, USA

C. R. Keeton⁺

Department of Physics and Astronomy, Rutgers University, 136 Frelinghuysen Road, Piscataway, New Jersey 08854, USA
(Received 18 October 2007; published 6 June 2008)

We model the massive dark object at the center of the Galaxy as a Schwarzschild black hole as well as Janis-Newman-Winicour naked singularities, characterized by the mass and scalar charge parameters, and study gravitational lensing (particularly time delay, magnification centroid, and total magnification) by them. We find that the lensing features are qualitatively similar (though quantitatively different) for Schwarzschild black holes, weakly naked, and marginally strongly naked singularities. However, the lensing characteristics of strongly naked singularities are qualitatively very different from those due to Schwarzschild black holes. The images produced by Schwarzschild black hole lenses and weakly naked and marginally strongly naked singularity lenses always have positive time delays. On the other hand, strongly naked singularity lenses can give rise to images with positive, zero, or negative time delays. In particular, for a large angular source position the direct image (the outermost image on the same side as the source) due to strongly naked singularity lensing always has a negative time delay. We also found that the scalar field decreases the time delay and increases the total magnification of images; this result could have important implications for cosmology. As the Janis-Newman-Winicour metric also describes the exterior gravitational field of a scalar star, naked singularities as well as scalar star lenses, if these exist in nature, will serve as more efficient cosmic telescopes than regular gravitational lenses.

DOI: [10.1103/PhysRevD.77.124014](https://doi.org/10.1103/PhysRevD.77.124014)

PACS numbers: 04.70.Bw, 04.20.Dw, 97.60.Lf, 98.62.Sb

I. INTRODUCTION

A naked (visible) singularity is defined as a spacetime singularity which can be seen by some observer and also lies to the future of some point of the spacetime [1]. The well-known weak cosmic censorship hypothesis (WCCH) of Penrose essentially states that, generically, spacetime singularities of physically realistic gravitational collapse are hidden within black holes [1,2]. The concept of visible singularities is objectionable to many scientists, as their existence is thought to have alarming astrophysical implications. On the other hand, a failure of the WCCH would give us the great opportunity to probe the extremely strong gravitational fields that will help in the discovery of the physical laws of quantum gravity. Despite many industrious efforts, we are still far from having a general proof (or disproof) of this hypothesis, and Penrose [1] expected that radically new mathematical techniques might be required for this purpose. As a proof or disproof of this hypothesis appears to be inordinately difficult, it may be easier to find a persuading counterexample to demonstrate that the hypothesis is not correct. Numerous diligent efforts have been put in this direction in the last four decades; however, we still do not have a single convincing counterexample to the

WCCH (see references in [1–3]). In a seminal review, Penrose [1] concluded that the question of cosmic censorship is still very much open and considered this to be possibly the most important unsolved problem in classical general relativity.

Given that we have neither a proof (or disproof) nor a convincing counterexample of the WCCH, it is important to explore whether or not this hypothesis could be tested observationally. To this end, Virbhadra *et al.* [4] introduced a theoretical research project using gravitational lensing phenomena, and encouraging results came out of that. Further, Virbhadra and Ellis [5] obtained a new gravitational lens equation that allows large deflection of light, and therefore it can be used to study strong gravitational field lensing. They used this lens equation to study the gravitational lensing due to light deflection close to the photon sphere of the supermassive “black hole” at the center of the Galaxy. They found that the presence of a photon sphere gives rise to a theoretically infinite sequence of highly demagnified images on both sides of the optical axis (the line joining the lens and the observer), and they termed these *relativistic images*. Virbhadra and Ellis [6] further extended the previous studies of Virbhadra *et al.* [4] in detail. They also organized the investigations by classifying naked singularities into two groups: *weakly naked* singularities (WNS) and *strongly naked* singularities (SNS). They modeled massive dark objects at the centers

*shwetket@yahoo.com

+keeton@physics.rutgers.edu

of a few galaxies as Schwarzschild black holes and Janis-Newman-Winicour weakly as well as strongly naked singularities, and studied gravitational lensing by them. The Schwarzschild black holes as well as weakly naked singularities have qualitatively similar lensing characteristics: both have one Einstein ring and no radial critical curves. On the other hand, the strongly naked singularities have qualitatively different lensing features; i.e., they give rise to two or zero Einstein rings and one radial critical curve. After publication of these results [4–7], there has been a growing curiosity in black hole lensing, and many interesting papers have appeared in last few years (see [8–19] and references therein).

In this paper, we study the time delay, magnification centroid, and total magnification of images due to gravitational lensing by Schwarzschild black holes and Janis-Newman-Winicour naked singularities. One of the most striking results in this paper is that the strongly naked singularities can give rise to images with negative time delays. As relativistic images are known to be extremely demagnified [5], we do not do computations for those in this paper. We use geometrized units (i.e., $G = 1$, $c = 1$) throughout this paper; however, we finally compute time delays in terms of minutes. We use MATHEMATICA [20] for computations.

II. LENS EQUATION, LIGHT DEFLECTION ANGLE, AND CLASSIFICATION OF NAKED SINGULARITIES

In this section, we write, in brief, some of the results obtained in previous papers [4–7,21,22] and refine the classification of naked singularities given in [6], because these are required for computations and analysis of results in this paper.

Virbhadra and Ellis [5] derived a gravitational lens equation that permits small as well as large bending angles of light, and that is given by

$$\tan\beta = \tan\theta - \alpha, \quad (1)$$

with

$$\alpha \equiv \frac{D_{ds}}{D_s} [\tan\theta + \tan(\hat{\alpha} - \theta)]. \quad (2)$$

D_s , D_{ds} , and D_d , respectively, are the observer-source, the lens-source, and the observer-lens distances. $\hat{\alpha}$ is the light bending angle. θ and β are, respectively, angular positions of an image and an unlensed source measured from the optical axis. (See Fig. 1 in [5].) The impact parameter $J = D_d \sin\theta$. For small angles, Eq. (1) reduces to the most well-known lens equation used for studying lensing in a weak gravitational field [23].

In circularly symmetric gravitational lensing, the magnification μ of an image is

$$\mu = \left(\frac{\sin\beta}{\sin\theta} \frac{d\beta}{d\theta} \right)^{-1}. \quad (3)$$

The tangential and radial magnifications are, respectively, expressed by

$$\mu_t = \left(\frac{\sin\beta}{\sin\theta} \right)^{-1} \quad \text{and} \quad \mu_r = \left(\frac{d\beta}{d\theta} \right)^{-1}. \quad (4)$$

The singularities in μ_t and μ_r in the lens plane give, respectively, *tangential critical curves* (TCCs) and *radial critical curves* (RCCs), and their corresponding values in the source plane are, respectively, known as the *tangential caustic* (TC) and *radial caustics* (RCs).

Virbhadra *et al.* [4] considered a general static and spherically symmetric spacetime described by the line element

$$ds^2 = B(r)dt^2 - A(r)dr^2 - D(r)r^2(d\vartheta^2 + \sin^2\vartheta d\varphi^2) \quad (5)$$

and calculated the deflection angle $\hat{\alpha}(r_0)$ and impact parameter $J(r_0)$ for a light ray with the closest distance of approach r_0 . These are given by

$$\hat{\alpha}(r_0) = 2 \int_{r_0}^{\infty} \left(\frac{A(r)}{D(r)} \right)^{1/2} \left[\left(\frac{r}{r_0} \right)^2 \frac{D(r)}{D(r_0)} \frac{B(r_0)}{B(r)} - 1 \right]^{-1/2} \times \frac{dr}{r} - \pi \quad (6)$$

and

$$J(r_0) = r_0 \sqrt{\frac{D(r_0)}{B(r_0)}}. \quad (7)$$

For $D(r) = 1$, Eqs. (6) and (7) yield the results obtained by Weinberg [24].

The most general static and spherically symmetric solution to the Einstein massless scalar equations was independently obtained by Janis, Newman, and Winicour, as well as Wyman [25]. As both solutions were available in different coordinates, they were not known to be the same until Virbhadra [21] showed the equivalence between the two by a coordinate transformation. As Janis, Newman, and Winicour obtained this solution about 13 years before Wyman, we prefer to call it the Janis-Newman-Winicour solution. Thus, the Janis-Newman-Winicour solution (characterized by constant and real parameters, the ADM mass M , and the scalar charge q) is expressed by the line element

$$ds^2 = \left(1 - \frac{b}{r} \right)^\nu dt^2 - \left(1 - \frac{b}{r} \right)^{-\nu} dr^2 - \left(1 - \frac{b}{r} \right)^{1-\nu} r^2 (d\vartheta^2 + \sin^2\vartheta d\varphi^2) \quad (8)$$

and the massless scalar field

$$\Phi = \frac{q}{b\sqrt{4\pi}} \ln\left(1 - \frac{b}{r}\right), \quad (9)$$

with

$$\nu = \frac{2M}{b} \quad \text{and} \quad b = 2\sqrt{M^2 + q^2}. \quad (10)$$

Obviously, $0 \leq \nu \leq 1$.

This solution is asymptotically Minkowskian and reduces to the Schwarzschild solution for $q = 0$ (i.e., $\nu = 1$). The Janis-Newman-Winicour solution has a *globally naked strong curvature singularity* at $r = b$ for all values of $q \neq 0$, and this solution is physically reasonable as it satisfies the weak energy condition [22]. Virbhadra *et al.* obtained the light deflection angle $\hat{\alpha}(r_0)$ for a large value of r_0 [see Eq. (24) in [4]]; we now reexpress that using Eq. (10), as follows:

$$\hat{\alpha}(r_0) = 2\nu\left(\frac{b}{r_0}\right) + \left[\nu(1 - 2\nu) + \pi\left(\nu^2 - \frac{1}{16}\right)\right]\left(\frac{b}{r_0}\right)^2 + \mathcal{O}\left(\frac{b}{r_0}\right)^3. \quad (11)$$

Virbhadra and Ellis [5] as well as Claudel *et al.* [7] gave two different definitions of a photon sphere in a static spherically symmetric spacetime. Both definitions gave the same results for a general static and spherically symmetric metric. Thus, according to both definitions, the Janis-Newman-Winicour spacetime has only one photon sphere and it is situated at the radial distance [6,7]

$$r_{\text{ps}} = \frac{b(1 + 2\nu)}{2}. \quad (12)$$

As $r = b$ is the curvature singularity, the photon sphere exists only for ν : $1/2 < \nu \leq 1$.

Defining

$$\rho = \frac{r}{b}, \quad \rho_0 = \frac{r_0}{b} \quad (13)$$

and using Eqs. (6)–(8), the deflection angle $\hat{\alpha}$ and the impact parameter J for a light ray in the Janis-Newman-Winicour spacetime are expressed in the form [4,6]

$$\begin{aligned} \hat{\alpha}(\rho_0) &= 2 \int_{\rho_0}^{\infty} \frac{d\rho}{\rho \sqrt{1 - \frac{1}{\rho}} \sqrt{\left(\frac{\rho}{\rho_0}\right)^2 \left(1 - \frac{1}{\rho}\right)^{1-2\nu} \left(1 - \frac{1}{\rho_0}\right)^{2\nu-1} - 1}} - \pi \end{aligned} \quad (14)$$

and

$$J(\rho_0) = 2M \frac{\rho_0}{\nu} \left(1 - \frac{1}{\rho_0}\right)^{(1-2\nu)/2}. \quad (15)$$

Obviously, Eq. (12) can now be reexpressed as

$$\rho_{\text{ps}} = \frac{(1 + 2\nu)}{2}. \quad (16)$$

Equation (15) along with the expression for the impact parameter, $J = D_d \sin\theta$, give

$$\sin\theta = \frac{2M}{D_d} \frac{\rho_0}{\nu} \left(1 - \frac{1}{\rho_0}\right)^{(1-2\nu)/2}. \quad (17)$$

The first derivative of the deflection angle $\hat{\alpha}$ with respect to θ is given by [4,6]

$$\frac{d\hat{\alpha}}{d\theta} = \hat{\alpha}'(\rho_0) \frac{d\rho_0}{d\theta}, \quad (18)$$

where

$$\frac{d\rho_0}{d\theta} = \frac{\nu\rho_0\left(1 - \frac{1}{\rho_0}\right)^{(1+2\nu)/2} \sqrt{1 - \frac{4}{\nu^2} \left(\frac{M}{D_d}\right)^2 \rho_0^2 \left(1 - \frac{1}{\rho_0}\right)^{1-2\nu}}}{\frac{M}{D_d}(2\rho_0 - 2\nu - 1)} \quad (19)$$

and

$$\hat{\alpha}'(\rho_0) = \frac{2\nu + 1 - 2\rho_0}{\rho_0^2 \left(1 - \frac{1}{\rho_0}\right)} \int_{\rho_0}^{\infty} \frac{(4\nu\rho - 2\nu - 1)d\rho}{(2\nu + 1 - 2\rho)^2 \rho \sqrt{1 - \frac{1}{\rho}} \sqrt{\left(\frac{\rho}{\rho_0}\right)^2 \left(1 - \frac{1}{\rho}\right)^{1-2\nu} \left(1 - \frac{1}{\rho_0}\right)^{2\nu-1} - 1}}. \quad (20)$$

The prime denotes the first derivative with respect to ρ_0 .

Virbhadra and Ellis [6] classified naked singularities in two groups: *Weakly naked singularities* are those which are contained within at least one photon sphere, whereas *strongly naked singularities* are those which are *not* covered within any photon spheres. Therefore, according to

this classification, the Janis-Newman-Winicour naked singularities are strongly naked for $0 \leq \nu \leq 1/2$ and weakly naked for $1/2 < \nu < 1$.

For Schwarzschild black holes ($\nu = 1$) as well as WNS ($1/2 < \nu < 1$), the deflection angle $\hat{\alpha}(\rho_0)$ monotonically increases with the decrease in the closest distance of

approach ρ_0 and $\hat{\alpha}(\rho_0) \rightarrow \infty$ as $\rho_0 \rightarrow \rho_{ps}$. As both have a qualitatively similar $\hat{\alpha}$ vs ρ_0 graph, their lensing features are also qualitatively similar [4,6]. However, Virbhadra and Ellis [6] missed noticing a point: Though there are no photon spheres for $\nu = 1/2$, the deflection angle behavior, according to Eq. (20), is similar to the cases of the Schwarzschild black hole and WNS; therefore, their gravitational lensing features will also be qualitatively the same. In view of this, we now prefer to term $\nu = 1/2$ and $0 \leq \nu < 1/2$ singularities, respectively, *marginally strongly naked singularities* (MSNS) and *strongly naked singularities*.

The mass parameter $M = 0$ in the Janis-Newman-Winicour solution describes the situation of a purely scalar field. We do not consider this case henceforth in this paper.

III. TIME DELAY, MAGNIFICATION CENTROID, AND TOTAL MAGNIFICATION

We consider light propagation in a static spherically symmetric spacetime described by the line element given by Eq. (5). The spherical symmetry of the spacetime allows us to consider, without loss of generality, null geodesics in the equatorial plane. We first obtain the time required for light to travel from a source at coordinates $\{r, \vartheta = \pi/2, \varphi = \varphi_1\}$ to the closest point of approach at coordinates $\{r_0, \vartheta = \pi/2, \varphi = \varphi_2\}$. Following the method used in [24], a straightforward calculation thus gives the time required for light to travel from r to r_0 (or r_0 to r), which is expressed by

$$t(r, r_0) = t(r_0, r) = \int_{r_0}^r \sqrt{\frac{A(r)/B(r)}{1 - \left(\frac{r_0}{r}\right)^2 \frac{B(r)}{B(r_0)} \frac{D(r_0)}{D(r)}}} dr. \quad (21)$$

$D(r) = 1$ in the above equation readily gives the result in [24]. Let \mathcal{R}_s and \mathcal{R}_o denote, respectively, the radial coordinates of the source and the observer measured from the center of mass of the deflector (lens). We now express these distances in terms of the constant parameter b (in the Janis-Newman-Winicour metric) by introducing

$$\mathcal{X}_s = \frac{\mathcal{R}_s}{b} \quad \text{and} \quad \mathcal{X}_o = \frac{\mathcal{R}_o}{b}. \quad (22)$$

The time delay $\tau(\rho_0)$ of light traveling from the source to the observer with the closest distance of approach ρ_0 is defined as the difference between the light travel time for the actual ray in the gravitational field of the lens (deflector) and the travel time for the straight path between the source and the observer in the absence of the lens (i.e., if there were no gravitational fields). As mentioned in Sec. II,

we do not consider the case of the purely scalar field in this paper; therefore, we assume that $\nu \neq 0$ (i.e., $M \neq 0$). Using Eqs. (8), (10), and (21), and the geometry of the lens diagram (see Fig. 1 in [5]), we obtain the following expression for the time delay in the Janis-Newman-Winicour spacetime:

$$\tau(\rho_0) = \frac{2M}{\nu} \left[\int_{\rho_0}^{\mathcal{X}_s} \frac{d\rho}{f(\rho)} + \int_{\rho_0}^{\mathcal{X}_o} \frac{d\rho}{f(\rho)} \right] - D_s \sec \beta \quad (23)$$

with

$$\mathcal{X}_s = \frac{\nu D_s}{2M} \sqrt{\left(\frac{D_{ds}}{D_s}\right)^2 + \tan^2 \beta}, \quad \mathcal{X}_o = \frac{\nu D_d}{2M}, \quad (24)$$

and

$$f(\rho) = \sqrt{\left(1 - \frac{1}{\rho}\right)^{2\nu} - \left(\frac{\rho_0}{\rho}\right)^2 \left(1 - \frac{1}{\rho}\right)^{4\nu-1} \left(1 - \frac{1}{\rho_0}\right)^{1-2\nu}}. \quad (25)$$

The first and second terms in Eq. (23) give, respectively, the travel time of the light from the source to the point of closest approach and from that point to the observer. The last term gives the light travel time from the source to the observer in the absence of any gravitational field.

We use Eq. (23) for computations in the next section. However, to see the behavior of the time delay function for a light ray traveling in the weak gravitational field far away from the lens, we carry out some analytical calculations following the method used in [15]. We obtain the time delay for images with large impact parameters. For given angular positions of the source and image, the time delay is given by

$$\tau(\theta, \beta) = \frac{1}{2} \frac{D_d D_s}{D_{ds}} \times \left[\left(2 - \frac{1}{\nu}\right) \theta_E^2 + \beta^2 - \theta^2 - \theta_E^2 \ln \left(\frac{\theta^2 D_d}{4 D_{ds}} \right) \right], \quad (26)$$

where

$$\theta_E = \sqrt{4M \frac{D_{ds}}{D_d D_s}} \quad (27)$$

is an approximate expression for angular radius of the Einstein ring of Schwarzschild lensing.

Equation (26) shows that, for $\nu < 1/2$ (SNS), the time delay of the direct image is negative for large β . This fact reflects in our computations in the next section.

We denote the time delay in the outermost image on the same side as the source (also called the direct image) by τ_{os} . The *differential time delay* $\Delta\tau$ of an image with time delay τ is defined by

$$\Delta\tau = \tau - \tau_{os}. \quad (28)$$

(When there is only one image on the same side as the source, we use the symbol τ_s instead of τ_{os} .) The differential time delay is thus measured in reference to the direct image. The *magnification-weighted centroid position* (also called *magnification centroid*) of images is defined by

$$\hat{\Theta} = \frac{\sum \theta_i |\mu_i|}{\sum |\mu_i|}. \quad (29)$$

Angles measured in clockwise and anticlockwise directions from the optical axis have positive and negative signs, respectively. Further, the *magnification centroid shift* of images is defined by

$$\Delta\hat{\Theta} = \beta - \hat{\Theta}. \quad (30)$$

The *total absolute magnification* (also simply called *total magnification*) μ_{tot} is defined by

$$\mu_{tot} = \sum |\mu_i|. \quad (31)$$

The magnification centroid and the total magnification are very important physical quantities in studying microlensing when the images are not resolved.

IV. COMPUTATIONS AND RESULTS

Virbhadra and Ellis [6] modeled massive dark objects (MDOs) at the centers of four different galaxies (including our Galaxy) as Schwarzschild black holes (SBH) and Janis-Newman-Winicour naked singularities, and studied point source gravitational lensing by them. They obtained the angular positions of critical curves and caustics, and studied the variation of magnification against the angular position of images near the critical curves. However, they did not study the time delay, magnification centroid, or the

total magnification; we accomplish these tasks in this paper.

We now consider the MDO at the center of our Galaxy with the recent values for the mass $M = 3.61 \times 10^6 M_\odot$ and the lens-observer distance $D_d = 7.62$ kpc [26]. As in [6], we take the lens (MDO) to be situated halfway between the source and the observer, i.e., $D_{ds}/D_s = 1/2$. We model the Galactic MDO as a Schwarzschild black hole, as well as Janis-Newman-Winicour WNS, MSNS, and SNS lenses. As we are considering updated values for M and D_d of the Galactic MDO, we first recompute critical curves and caustics, and their corresponding deflection angles of the light ray for several values of ν . Then for given values of β , using MATHEMATICA we numerically solve the lens equation (1) and obtain image positions. For these images, we compute numerically other physical quantities, such as deflection angles, time delays, and magnifications. Our numerical computations are exact in the sense that we do not take weak or strong field limits. For continuity and clarity in the analysis of the results, we will also mention some results from [4,6] in the present and next sections of this paper. All tables are put in the Appendix.

As shown in Table I, there is only one Einstein ring and no RCC for the case of SBH ($\nu = 1$), WNS ($\nu = 0.9, 0.8, 0.7, 0.6$), and MSNS ($\nu = 0.5$). The angular positions of the Einstein rings decrease very slowly with a decrease in the value of ν [equivalently, an increase in the value of $(q/M)^2$]. In the case of SNS lensing ($0 < \nu < 1/2$), there are two situations: there is always one RCC; however, there can be two (for example, for $\nu = 0.4, 0.3$, etc.) or zero Einstein rings (for example, for $\nu = 0.001$ and any lower values of ν). For the cases of double Einstein rings, the angular radii of the outer and inner rings, respectively, decrease and increase with a decrease in the value of ν . For a detailed analysis of these RCCs and TCCs, see [6].

We now compute image positions, the corresponding deflection angles of light, magnifications, time delays, and differential time delays for several values of the angular source position for different values of $\nu = 1$ (SBH), $\nu = 0.7$ (WNS), $\nu = 0.5$ (MSNS), and $\nu = 0.04, 0.02, 0.001$ (SNS). Though we give only a few data in the tables, we have computed and used many more data points for the figures.

The gravitational lensing effects due to the SBH, WNS, and MSNS are qualitatively similar, though they differ quantitatively by small values (see Tables II, III, and IV and Fig. 1). For each case, there are two images, one on each side of the optical axis. As the source moves away from the optical axis, the image on the same side as the source (i.e., the direct image) moves away from the axis, whereas the image on the opposite side of the lens from the source moves toward the axis. The absolute magnification of both images decreases. For a given value of ν , with an increase in the angular position of the source, the time delay of the image on the same side as the source de-

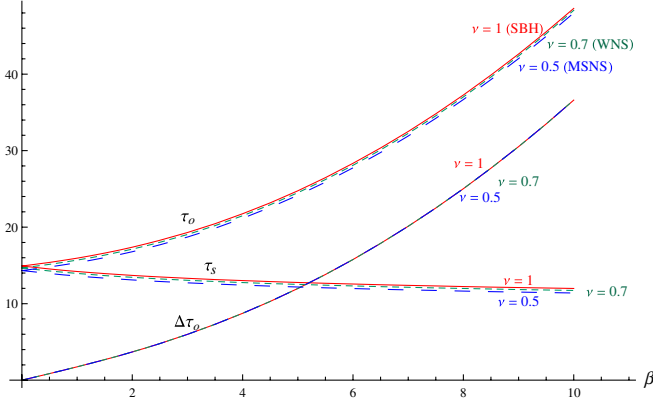


FIG. 1 (color online). The *time delays* of the images on the opposite side from the source τ_o , the same side as the source τ_s , and the *differential time delay* of the images on the opposite side from the source $\Delta\tau_o$ are plotted against the angular source position β for $\nu = 1$ (SBH), $\nu = 0.7$ (WNS), and $\nu = 0.5$ (MSNS). $M/D_d \approx 2.26 \times 10^{-11}$ and $D_{ds}/D_s = 1/2$. The time delays as well as differential time delays are expressed in minutes, whereas the angular source position is given in arcseconds.

creases, whereas the time delay and differential time delay of the image on the opposite side from the source increase. The rate of decrease in the time delay of the image on the same side as the source is much slower than the rate of increase in the time delay of the image on the opposite side from the source. For any given value of the angular source position, the time delays of both images and the differential time delay of the image on the opposite side from the source decrease with a decrease in the value of ν [equivalently, an increase in $(q/M)^2$].

Gravitational lensing by a SNS is qualitatively *very* different from lensing by SBH, WNS, or MSNS (see Tables V, VI, VII, VIII, and IX and Figs. 2–4). For $\nu = 0.04$ and 0.02 , when the lens components (the source, lens, and observer) are perfectly (or nearly) aligned, there are two concentric Einstein rings (the inner ring much fainter than the outer one). As the alignment is broken, the two Einstein rings break into four images, two images on each side of the optical axis. The time delay of the direct image decreases with an increase in β . For $\nu = 0.04$, the time delay of the direct image is positive for small β and negative for large β ; however, the time delays for other images are positive for all values of β . On the other hand, for $\nu = 0.02$, the time delay of the direct image is always negative; however, the other three images have negative time delays for small β and positive for large β , passing through a zero time delay point.

For given values of ν and β , the time delays of the images are in the following decreasing order: the inner image on the opposite side from the source, the inner image on the same side as the source, the outer image on the opposite side from the source, and the direct image.

However, the absolute magnifications of the images are not in the exact reverse sequence; they are rather in the following decreasing order: the direct image, the outer image on the opposite side from the source, the inner image on the opposite side from the source, and the inner image on the same side as the source. The differential time delays are always positive. It is worth emphasizing that the negative and positive time delays are, respectively, not necessarily due to negative and positive bending angles. A light ray with a positive deflection angle may give rise to a positive or negative time delay, and the same is true for a light ray with a negative deflection angle. If β increases, the angular separation between the images on the same side as the source increases (the inner and outer images move, respectively, toward and away from the optical axis). However, the angular separation between the images on the opposite side from the source decreases (the outer and inner images move, respectively, toward and away from the optical axis), and for some value of β these two images coalesce to form one highly magnified image; for example, for $\nu = 0.02$, the angular positions of the source and image are $\beta \approx 210.2934$ arcsec (RC) and $\theta \approx -0.004591$ arcsec (RCC), respectively. The opposite signs on these two values show that the RCC and RC are on opposite sides of the optical axis (see Table I). For further increase in β , there are no images on the opposite side from the source.

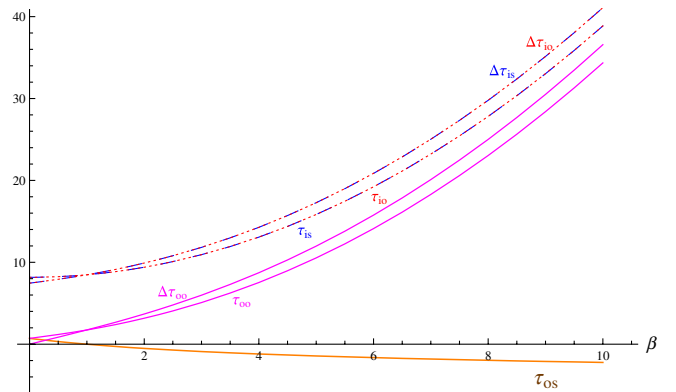


FIG. 2 (color online). The *time delays* of the outer image on the same side as the source τ_{os} , the inner image on the same side as the source τ_{is} , the inner image on the opposite side from the source τ_{io} , and the outer image on the opposite side from the source τ_{oo} are plotted against the angular source position β for $\nu = 0.04$ (SNS). Also, the *differential time delays* of the inner image on the same side as the source $\Delta\tau_{is}$, the inner image on the opposite side from the source $\Delta\tau_{io}$, and the outer image on the opposite side from the source $\Delta\tau_{oo}$ are plotted against β for the same value of ν . $D_{ds}/D_s = 1/2$ and $M/D_d \approx 2.26 \times 10^{-11}$. The time delays as well as differential time delays are in minutes, whereas the angular source position is expressed in arcseconds.

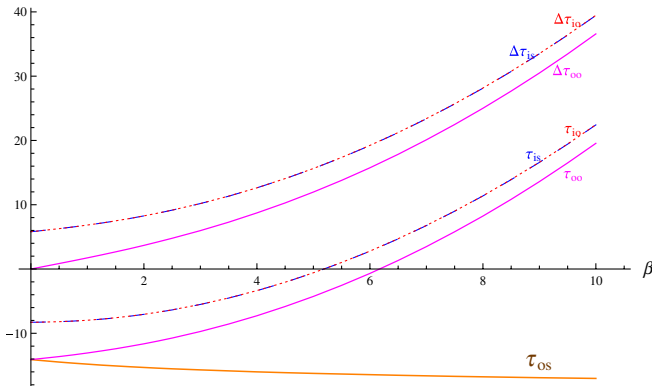


FIG. 3 (color online). The *time delays* of the direct image τ_{os} , the inner image on the same side as the source τ_{is} , the inner image on the opposite side from the source τ_{io} , and the outer image on the opposite side from the source τ_{oo} are plotted against the angular source position β for $\nu = 0.02$ (SNS). The *differential time delays* of the inner image on the same side as the source $\Delta\tau_{is}$, the inner image on the opposite side from the source $\Delta\tau_{io}$, and the outer image on the opposite side from the source $\Delta\tau_{oo}$ are plotted against β for the same value of ν . The angular source position is expressed in arcseconds, whereas the time delays as well as differential time delays are shown in minutes. $M/D_d \approx 2.26 \times 10^{-11}$ and $D_{ds}/D_s = 1/2$.

For $\nu = 0.001$, see Table IX and Fig. 4. If the lens components are aligned, there are no Einstein rings. Also, for small values of β , there are no images on either side of the optical axis. For $\beta \approx 0.808397$ arcsec (RC), there is a highly magnified image at the angular position $\theta \approx 1.115015$ arcsec (RCC). The signs on RC and RCC being the same implies that this image appears on the same side as the source. As β further increases, the image splits into two, and the inner and outer (direct) images move toward and away from the optical axis, respectively; the magnification of the inner image decreases much faster than the outer one. The time delay of the direct image for this case is always negative and decreases slowly with an increase in β . The time delay of the inner image, however, is negative for small β and positive for large β , passing through the zero time delay for a certain value of β . The increase rate of the time delay of the inner image is much higher than the decrease rate of the time delay of the direct image. For the inner image, the deflection angles are positive and negative, respectively, for small and large values of β ; however, for the direct image it is always positive. As for other cases already discussed, the differential time delay of the inner image is always positive.

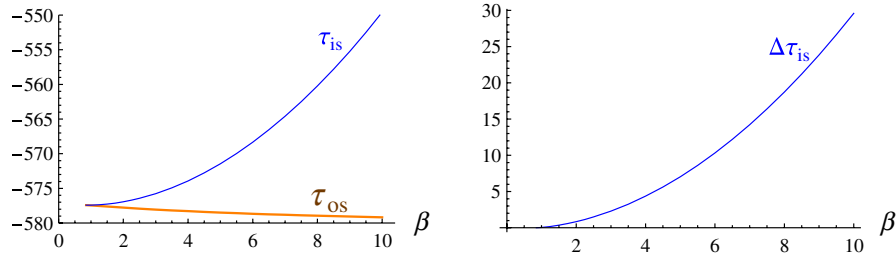


FIG. 4 (color online). The *time delays* of the outer image on the same side as the source τ_{os} and the inner image on the same side as the source τ_{is} are plotted against the angular source position β for $\nu = 0.001$ (SNS); see the left figure. The *differential time delay* of the inner image on the same side as the source $\Delta\tau_{is}$ is plotted against β (right figure). The time delays as well as the differential time delay and the angular source position are, respectively, given in minutes and arcseconds. $D_{ds}/D_s = 1/2$ and $M/D_d \approx 2.26 \times 10^{-11}$.

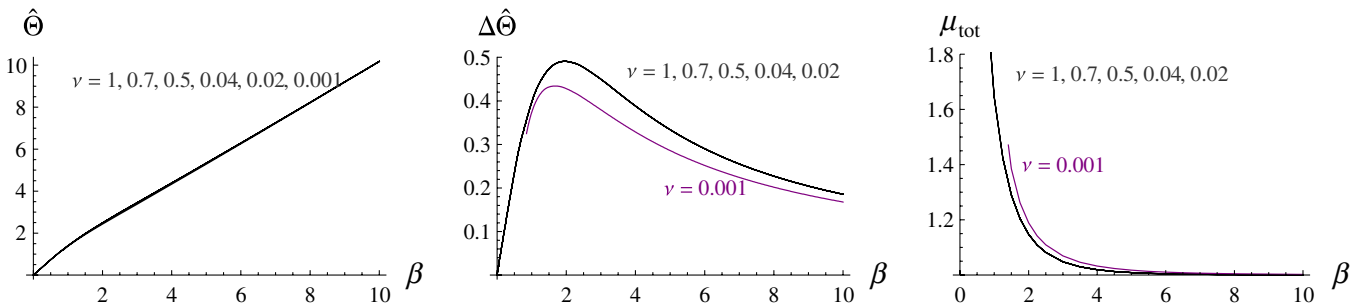


FIG. 5 (color online). The *magnification centroid* $\hat{\theta}$, the *magnification centroid shift* $\Delta\hat{\theta}$, and the *total magnification* μ_{tot} are plotted against the angular source position β for $\nu = 1$ (SBH), $\nu = 0.7$ (WNS), $\nu = 0.5$ (MSNS), and $\nu = 0.04, 0.02, 0.001$ (SNS). $D_{ds}/D_s = 1/2$ and $M/D_d \approx 2.26 \times 10^{-11}$. $\hat{\theta}$, $\Delta\hat{\theta}$, and β are expressed in arcseconds.

We now compute the magnification centroid, the magnification centroid shift, and the total magnification for $\nu = 1$ (SBH), $\nu = 0.7$ (WNS), $\nu = 0.5$ (MSNS), and $\nu = 0.04, 0.02, 0.001$ (SNS) for several values of β (see Tables X, XI, and XII). We then plot these quantities against β (see Fig. 5). For a fixed value of ν , the magnification centroid increases with an increase in β . For small values of β , the graph is bulged up and then tends to become straight as β increases. For a fixed value of β , the magnification centroid decreases with a decrease in ν [i.e., an increase in $(q/M)^2$]; the decrease is, however, too small for these five graphs to appear resolved even if these were plotted on an entire page. As β increases, the magnification centroid shift first increases, reaches a maximum value, and then starts decreasing to the limiting value zero. For a given value of β , the magnification centroid shift decreases with a decrease in the value of ν . For a given value of ν , the total magnification is, as expected, very high for small β , and it decreases to the limiting value of 1, as β increases. For any given value of β , however, the total magnification increases with a decrease in the value of ν . Thus, the presence of scalar charge helps increase the total magnification. This would provide a modest increase in the likelihood of observing lensing by SgrA* (see [27] and references therein).

V. DISCUSSION AND CONCLUSION

The naked singularities are classified in three categories: WNS, MSNS, and SNS. We modeled the Galactic MDO as the SBH, and Janis-Newman-Winicour WNS, MSNS, and SNS lenses, and studied point source gravitational lensing by them. We found that the gravitational lensing effects due to the SBH, WNS, and MSNS are qualitatively similar (but these differ slightly quantitatively) to each other; however, they differ qualitatively from SNS lensing. Therefore, it will be easier to observationally differentiate a SNS (compared to a WNS or a MSNS) from a SBH.

SBH, WNS, and MSNS lensing.—These do not give rise to any radial caustics; however, they do produce one Einstein ring when the lens components are aligned (i.e., $\beta = 0$). When β increases, the Einstein ring splits into two images, one on each side of the optical axis. The time delays for both images are positive for all values of β . For a given value of β , a decrease in ν , i.e., an increase in $(q/M)^2$, decreases the absolute angular image positions, time delays, magnification centroid, and magnification centroid shift; however, it increases the total magnification of images. The differences are, however, very small. The deflection angle $\hat{\alpha}$ becomes unboundedly large as the impact parameter $J \rightarrow J_{\text{ps}}$ for the SBH and WNS [6].

SNS lensing.—There are two types of lensing in this category. In the first, for example for the case of $\nu = 0.02$, there are double concentric Einstein rings (when

$\beta = 0$) and one radial critical curve (when $\beta \approx 210.2934$ arcsec). As the angular position of the source increases from the alignment position of the lens components (i.e., $\beta = 0$), the two Einstein rings “break” into four images, giving two images on each side of the optical axis. The separation between images on the same and opposite sides from the source, respectively, increases and decreases as β increases, and eventually the two images on the opposite side from the source coalesce to form a single, highly magnified image. For any further increase in β , there are only two images on the same side as the source. For the second category of SNS lensing, for example for $\nu = 0.001$, there is one RC; however, there is no Einstein ring when $\beta = 0$. Moreover, there is no image for small values of β . As β increases, a highly magnified image (RCC) first appears on the same side as the source. A further increase in β splits this into two images, and the separation between them keeps increasing (both images remaining on the same side as the source). The time delay of images of SNS lensing may be positive, zero, or negative depending on the values of ν and β . However, the time delay of a direct image is negative for any SNS lensing if β is large. As shown in [6], the deflection angle $\hat{\alpha}$ approaches $-\pi$ as the impact parameter approaches its minimum value of zero. Therefore, if a light ray with a very small impact parameter is sent toward a SNS, it will “bounce”; however, it remains to be computed whether or not the “reflected” light has enough magnification to be observed by present instruments or by those likely to be available in the near future. This may serve as a crucial test for the existence of SNS.

All the images produced by the Galactic MDO (modeled as a Schwarzschild black hole and as naked singularity lenses) may be resolved from each other by observational facilities available in the near future. Therefore, the results of the magnification centroid and total magnification may not be needed. However, our studies help us understand the role of the scalar field on the magnification centroid and total magnification, which could be useful while studying gravitational lensing by exotic dark objects having rather small values of M/D_d and D_{ds}/D_s . For several reasons, gravitational lensing observations in the vicinity of a galactic center are very difficult (see [5] for details). However, we expect that improved observational facilities in the future will overcome these difficulties.

The existence of a photon sphere covering a gravitational lens is a sufficient (but not necessary) condition for the occurrence of relativistic images. The SBH as well as WNS are contained inside a photon sphere, and both give rise to relativistic images. The MSNS also produces relativistic images, even though it is not covered by a photon sphere. The relativistic images are transient and extremely demagnified, and therefore their observations do not seem to be feasible in the near future [5]. For this reason, we did not do computations for relativistic images in this paper.

In lensing observations, what has been measured until now is the differential time delay (not the time delay itself). However, there are scenarios in which it is conceivable that the time delay can be measured. Suppose a pulsar orbits a compact object (another neutron star, or a black hole, or a naked singularity). The pulses provide a precise clock that makes it possible to measure changes in the light travel time as the pulsar moves through its orbit. In particular, the pulse arrival times can be analyzed to determine the lensing time delay. Rafikov and Lai [28] have discussed this possibility for binary pulsar systems, such as J0737-3039. The same idea would apply to a pulsar orbiting the massive dark object at the center of our Galaxy. Thus, it is possible to test our fascinating results of negative time delay.

Naked singularity lensing gives rise to images of smaller time delay and stronger total magnification than black hole lensing. Therefore, if naked singularities indeed exist in nature, then these will serve as *better cosmic telescopes* and will help probe the Universe more efficiently. The results obtained in this paper also help us understand the effects of the scalar field on gravitational lensing, which could have valuable implications for research in cosmology.

The Janis-Newman-Winicour metric also describes the exterior gravitational field of a scalar star. Therefore, re-

sults obtained in this paper for naked singularities are also applicable to scalar stars. The scalar star, however, must be compact enough for the images not to be obstructed.

The metric we considered in this paper may or may not be physically realistic. However, gravitational lensing studies with this metric serve as stepping stones to understand the distinctive lensing features of black holes and naked singularities. Rauch and Blandford's [29] pioneering work on Kerr black hole lensing has been recently followed up by many researchers (see [30] and references therein). It would be indeed of great astrophysical significance to obtain distinguishing *qualitative* lensing characteristics of Kerr black holes and Kerr naked singularities, so that the weak cosmic censorship hypothesis could be tested observationally without any ambiguity.

ACKNOWLEDGMENTS

Thanks are due to J. M. Aguirregabiria for some helpful correspondence related to MATHEMATICA and to E. Linder for a careful reading of the manuscript.

APPENDIX

Tables I, II, III, IV, V, VI, VII, VIII, IX, X, XI, and XII are given in this section.

TABLE I. Critical curves and caustics due to gravitational lensing by the Galactic MDO modeled as a Schwarzschild black hole, and as weakly, marginally strongly, and strongly naked singularities. θ_E , θ_r , and β_r denote, respectively, the angular positions of the tangential critical curves (Einstein rings), radial critical curves, and radial caustics, whereas $\hat{\alpha}$ stands for the corresponding light deflection angles. (a) The lens has mass $M = 3.61 \times 10^6 M_\odot$ and the distance $D_d = 7.62$ kpc so that $M/D_d \approx 2.26 \times 10^{-11}$. The ratio of the source-lens distance to the source-observer distance, i.e., $D_{ds}/D_s = 1/2$. All angular positions are given in arcseconds.

ν	Inner Einstein ring		Radial critical curve and caustic			Outer Einstein ring	
	θ_E	$\hat{\alpha}$	θ_r	$\hat{\alpha}$	β_r	θ_E	$\hat{\alpha}$
1.0	×	×	×	×	×	1.388 176	2.776 352
0.9	×	×	×	×	×	1.388 176	2.776 352
0.8	×	×	×	×	×	1.388 176	2.776 352
0.7	×	×	×	×	×	1.388 176	2.776 351
0.6	×	×	×	×	×	1.388 175	2.776 351
0.5	×	×	×	×	×	1.388 175	2.776 350
0.4	0.000 012	0.000 024	-0.000 019	286 883.8	252 026.7	1.388 174	2.776 348
0.3	0.000 015	0.000 030	-0.000 026	121 357.9	66 413.69	1.388 172	2.776 343
0.2	0.000 027	0.000 054	-0.000 051	46 469.19	23 533.19	1.388 165	2.776 330
0.1	0.000 095	0.000 191	-0.000 188	10 759.36	5383.343	1.388 131	2.776 262
0.05	0.000 371	0.000 741	-0.000 739	2641.816	1320.961	1.387 993	2.775 986
0.04	0.000 577	0.001 154	-0.001 151	1687.159	843.5924	1.387 890	2.775 780
0.03	0.001 023	0.002 046	-0.002 043	947.4574	473.7291	1.387 667	2.775 334
0.02	0.002 297	0.004 593	-0.004 591	420.5955	210.2934	1.387 029	2.774 057
0.01	0.009 176	0.018 352	-0.018 345	105.0746	52.518 93	1.383 568	2.767 135
0.005	0.036 717	0.073 434	-0.073 177	26.263 79	13.058 72	1.369 456	2.738 911
0.004	0.057 426	0.114 853	-0.113 887	16.807 84	8.290 033	1.358 574	2.717 148
0.003	0.102 472	0.204 944	-0.199 693	9.450 634	4.525 624	1.334 103	2.668 206
0.002	0.236 134	0.472 268	-0.420 122	4.166 782	1.663 269	1.254 966	2.509 932
0.001	×	×	1.115 015	0.613 237	0.808 397	×	×

TABLE II. Image positions due to lensing by the Galactic MDO modeled as a Schwarzschild black hole ($\nu = 1$), and their respective bending angles, magnifications, time delays, and differential time delays. (a) θ and $\hat{\alpha}$, respectively, stand for the angular positions of images and their corresponding deflection angles. μ , τ , and $\Delta\tau$ represent the magnification, time delay, and differential time delay of the images, respectively. (b) The subscripts s and o on the symbols, respectively, denote for the images on the same and opposite side from the source. (c) The same as (a) of Table I.

β	Image on the opposite side from the source					Image on the same side as the source			
	θ_o	$\hat{\alpha}_o$	μ_o	τ_o	$\Delta\tau_o$	θ_s	$\hat{\alpha}_s$	μ_s	τ_s
0	-1.388 176	2.776 352	\times	14.922 09	0	1.388 176	2.776 352	\times	14.922 09
10^{-5}	-1.388 171	2.776 362	-69 407.97	14.922 10	0.000 017	1.388 181	2.776 342	69 408.97	14.922 08
10^{-3}	-1.387 676	2.777 353	-693.5848	14.922 94	0.001 706	1.388 676	2.775 353	694.5848	14.921 24
10^{-1}	-1.339 077	2.878 153	-6.454 348	15.008 95	0.170 636	1.439 076	2.678 152	7.454 345	14.838 31
2	-0.710 863	5.421 726	-0.073 840	17.380 33	3.687 537	2.710 855	1.421 709	1.073 838	13.692 80
4	-0.434 558	8.869 117	-0.009 696	21.747 18	8.734 391	4.434 547	0.869 094	1.009 695	13.012 79
6	-0.305 617	12.611 23	-0.002 355	28.338 06	15.771 41	6.305 604	0.611 208	1.002 354	12.566 65
8	-0.234 044	16.468 09	-0.000 809	37.268 52	25.029 69	8.234 031	0.468 062	1.000 808	12.238 82
10	-0.189 138	20.378 28	-0.000 345	48.587 14	36.606 42	10.189 12	0.378 250	1.000 345	11.980 72

TABLE III. Image positions due to lensing by the Galactic MDO modeled as a weakly naked singularity ($\nu = 0.7$), and their respective bending angles, magnifications, time delays, and differential time delays. (a) The same as (a) and (b) of Table II. (b) The same as (a) of Table I.

β	Image on the opposite side from the source					Image on the same side as the source			
	θ_o	$\hat{\alpha}_o$	μ_o	τ_o	$\Delta\tau_o$	θ_s	$\hat{\alpha}_s$	μ_s	τ_s
0	-1.388 176	2.776 351	\times	14.668 36	0	1.388 176	2.776 351	\times	14.668 36
10^{-5}	-1.388 171	2.776 361	-69 407.97	14.668 36	0.000 017	1.388 181	2.776 341	69 408.97	14.668 35
10^{-3}	-1.387 676	2.777 352	-693.5848	14.669 21	0.001 706	1.388 676	2.775 352	694.5848	14.667 50
10^{-1}	-1.339 076	2.878 152	-6.454 347	14.755 21	0.170 636	1.439 076	2.678 151	7.454 345	14.584 57
2	-0.710 862	5.421 724	-0.073 840	17.126 60	3.687 536	2.710 855	1.421 709	1.073 838	13.439 06
4	-0.434 558	8.869 115	-0.009 696	21.493 45	8.734 389	4.434 547	0.869 094	1.009 695	12.759 06
6	-0.305 616	12.611 23	-0.002 355	28.084 32	15.771 41	6.305 604	0.611 208	1.002 354	12.312 92
8	-0.234 043	16.468 09	-0.000 809	37.014 78	25.029 69	8.234 031	0.468 062	1.000 808	11.985 09
10	-0.189 137	20.378 27	-0.000 345	48.333 40	36.606 42	10.189 12	0.378 250	1.000 345	11.726 98

TABLE IV. Image positions due to lensing by the Galactic MDO modeled as a marginally strongly naked singularity ($\nu = 0.5$), and their respective bending angles, magnifications, time delays, and differential time delays. (a) The same as (a) and (b) of Table II. (b) The same as (a) of Table I.

β	Image on the opposite side from the source					Image on the same side as the source			
	θ_o	$\hat{\alpha}_o$	μ_o	τ_o	$\Delta\tau_o$	θ_s	$\hat{\alpha}_s$	μ_s	τ_s
0	-1.388 175	2.776 350	\times	14.330 04	0	1.388 175	2.776 350	\times	14.330 04
10^{-5}	-1.388 170	2.776 360	-69 407.97	14.330 05	0.000 017	1.388 180	2.776 340	69 408.97	14.330 03
10^{-3}	-1.387 675	2.777 350	-693.5848	14.330 89	0.001 706	1.388 675	2.775 350	694.5848	14.329 19
10^{-1}	-1.339 075	2.878 150	-6.454 347	14.416 89	0.170 636	1.439 075	2.678 150	7.454 345	14.246 26
2	-0.710 861	5.421 721	-0.073 840	16.788 28	3.687 533	2.710 854	1.421 708	1.073 838	13.100 75
4	-0.434 556	8.869 112	-0.009 696	21.155 13	8.734 385	4.434 547	0.869 094	1.009 695	12.420 74
6	-0.305 614	12.611 23	-0.002 354	27.746 00	15.771 40	6.305 604	0.611 208	1.002 354	11.974 60
8	-0.234 041	16.468 08	-0.000 809	36.676 46	25.029 68	8.234 031	0.468 062	1.000 808	11.646 78
10	-0.189 135	20.378 27	-0.000 345	47.995 08	36.606 40	10.189 12	0.378 250	1.000 345	11.388 67

TABLE V. Image positions on the same side as the source due to lensing by the Galactic MDO modeled as a strongly naked singularity ($\nu = 0.04$), and their respective bending angles, magnifications, time delays, and differential time delays. (a) The same as (a) of Table II. (b) The subscripts is and os on the symbols, respectively, denote for the inner and outer images on the same side as the source. (c) The same as (a) of Table I.

β	Inner image on the same side as the source					Outer image on the same side as the source			
	θ_{is}	$\hat{\alpha}_{is}$	μ_{is}	τ_{is}	$\Delta\tau_{is}$	θ_{os}	$\hat{\alpha}_{os}$	μ_{os}	τ_{os}
0	0.000 577	0.001 154	\times	8.164 602	7.452 653	1.387 890	2.775 780	\times	0.711 949
10^{-5}	0.000 577	0.001 134	-9.9×10^{-6}	8.164 602	7.452 662	1.387 895	2.775 770	69 408.97	0.711 940
10^{-3}	0.000 577	-0.000 846	-9.9×10^{-8}	8.164 602	7.453 505	1.388 390	2.774 780	694.5849	0.711 097
10^{-1}	0.000 577	-0.198 846	-9.9×10^{-10}	8.167 637	7.539 395	1.438 800	2.677 600	7.454 397	0.628 242
2	0.000 577	-3.998 847	-4.9×10^{-11}	9.391 988	9.908 244	2.710 736	1.421 472	1.073 866	-0.516 256
4	0.000 576	-7.998 848	-2.5×10^{-11}	13.075 56	14.271 26	4.434 496	0.868 992	1.009 705	-1.195 693
6	0.000 576	-11.998 85	-1.6×10^{-11}	19.215 33	20.856 81	6.305 578	0.611 155	1.002 358	-1.641 480
8	0.000 576	-15.998 85	-1.2×10^{-11}	27.811 28	29.780 34	8.234 015	0.468 030	1.000 810	-1.969 056
10	0.000 575	-19.998 85	-9.7×10^{-12}	38.863 43	41.090 40	10.189 11	0.378 229	1.000 346	-2.226 996

TABLE VI. Image positions on the opposite side from the source due to lensing by the Galactic MDO modeled as a strongly naked singularity ($\nu = 0.04$), and their respective bending angles, magnifications, time delays, and differential time delays. (a) The same as (a) of Table II. (b) The subscripts io and oo on the symbols, respectively, denote for the inner and outer images on the opposite side from the source. (c) The same as (a) of Table I.

β	Outer image on the opposite side from the source					Inner image on the opposite side from the source				
	θ_{oo}	$\hat{\alpha}_{oo}$	μ_{oo}	τ_{oo}	$\Delta\tau_{oo}$	θ_{io}	$\hat{\alpha}_{io}$	μ_{io}	τ_{io}	$\Delta\tau_{io}$
0	-1.387 890	2.775 780	\times	0.711 949	0	-0.000 577	0.001 154	\times	8.164 602	7.452 653
10^{-5}	-1.387 885	2.775 790	-69 407.97	0.711 957	0.000 017	-0.000 577	0.001 174	9.9×10^{-6}	8.164 602	7.452 662
10^{-3}	-1.387 390	2.776 780	-693.5848	0.712 801	0.001 704	-0.000 577	0.003 154	9.9×10^{-8}	8.164 603	7.453 506
10^{-1}	-1.338 780	2.877 560	-6.454 297	0.798 725	0.170 483	-0.000 577	0.201 154	9.9×10^{-10}	8.167 708	7.539 465
2	-0.710 409	5.420 818	-0.073 812	3.168 027	3.684 283	-0.000 577	4.001 155	5.0×10^{-11}	9.393 405	9.909 661
4	-0.434 037	8.868 073	-0.009 686	7.531 250	8.726 943	-0.000 578	8.001 155	2.5×10^{-11}	13.078 40	14.274 09
6	-0.305 070	12.610 14	-0.002 351	14.116 91	15.758 39	-0.000 578	12.001 16	1.7×10^{-11}	19.219 58	20.861 06
8	-0.233 486	16.466 97	-0.000 807	23.040 51	25.009 57	-0.000 578	16.001 16	1.2×10^{-11}	27.816 95	29.786 01
10	-0.188 575	20.377 14	-0.000 344	34.350 62	36.577 58	-0.000 579	20.001 16	1.0×10^{-11}	38.870 51	41.097 48

TABLE VII. Image positions on the same side as the source due to lensing by the Galactic MDO modeled as a strongly naked singularity ($\nu = 0.02$), and their respective bending angles, magnifications, time delays, and differential time delays. (a) The same as (a) of Table II. (b) The same as (b) of Table V. (c) The same as (a) of Table I.

β	Inner image on the same side as the source					Outer image on the same side as the source			
	θ_{is}	$\hat{\alpha}_{is}$	μ_{is}	τ_{is}	$\Delta\tau_{is}$	θ_{os}	$\hat{\alpha}_{os}$	μ_{os}	τ_{os}
0	0.002 297	0.004 593	\times	-8.271 824	5.808 667	1.387 029	2.774 057	\times	-14.080 49
10^{-5}	0.002 297	0.004 573	-6.3×10^{-4}	-8.271 824	5.808 675	1.387 034	2.774 047	69 409.04	-14.080 50
10^{-3}	0.002 297	0.002 593	-6.3×10^{-6}	-8.271 825	5.809 517	1.387 529	2.773 058	694.5857	-14.081 34
10^{-1}	0.002 296	-0.195 407	-6.3×10^{-8}	-8.268 894	5.895 250	1.437 970	2.675 940	7.454 558	-14.164 14
2	0.002 291	-3.995 418	-3.1×10^{-9}	-7.046 546	8.261 433	2.710 378	1.420 757	1.073 949	-15.307 98
4	0.002 286	-7.995 428	-1.5×10^{-9}	-3.365 073	12.622 05	4.434 343	0.868 685	1.009 733	-15.987 12
6	0.002 280	-11.995 44	-1.0×10^{-9}	2.772 596	19.205 37	6.305 498	0.610 996	1.002 370	-16.432 77
8	0.002 275	-15.995 45	-7.5×10^{-10}	11.36 646	28.126 74	8.233 968	0.467 935	1.000 816	-16.760 28
10	0.002 270	-19.995 46	-5.9×10^{-10}	22.416 52	39.434 66	10.189 08	0.378 166	1.000 349	-17.018 14

TABLE VIII. Image positions on the opposite side from the source due to lensing by the Galactic MDO modeled as a strongly naked singularity ($\nu = 0.02$), and their respective bending angles, magnifications, time delays, and differential time delays. (a) The same as (a) of Table II. (b) The same as (b) of Table VI. (c) The same as (a) of Table I.

β	Outer image on the opposite side from the source					Inner image on the opposite side from the source				
	θ_{oo}	$\hat{\alpha}_{oo}$	μ_{oo}	τ_{oo}	$\Delta\tau_{oo}$	θ_{io}	$\hat{\alpha}_{io}$	μ_{io}	τ_{io}	$\Delta\tau_{io}$
0	-1.387 029	2.774 057	×	-14.080 49	0	-0.002 297	0.004 593	×	-8.271 824	5.808 667
10^{-5}	-1.387 024	2.774 067	-69 408.04	-14.080 48	0.000 017	-0.002 297	0.004 613	6.3×10^{-4}	-8.271 824	5.808 675
10^{-3}	-1.386 528	2.775 057	-693.5853	-14.079 64	0.001 703	-0.002 297	0.006 593	6.3×10^{-6}	-8.271 822	5.809 520
10^{-1}	-1.337 888	2.875 776	-6.454 149	-13.993 77	0.170 377	-0.002 297	0.204 594	6.3×10^{-8}	-8.268 612	5.895 533
2	-0.709 041	5.418 082	-0.073 730	-11.625 81	3.682 166	-0.002 302	4.004 604	3.2×10^{-9}	-7.040 905	8.267 074
4	-0.432 460	8.864 920	-0.009 657	-7.264 419	8.722 705	-0.002 308	8.004 615	1.6×10^{-9}	-3.353 791	12.633 33
6	-0.303 414	12.606 83	-0.002 339	-0.680 750	15.752 03	-0.002 313	12.004 63	1.1×10^{-9}	2.789 520	19.222 29
8	-0.231 793	16.463 59	-0.000 801	8.240 791	25.001 07	-0.002 319	16.004 64	8.2×10^{-10}	11.389 03	28.149 30
10	-0.186 860	20.373 72	-0.000 341	19.548 80	36.566 94	-0.002 325	20.004 65	6.7×10^{-10}	22.444 73	39.462 87

TABLE IX. Image positions on the same side as the source due to lensing by the Galactic MDO modeled as a strongly naked singularity ($\nu = 0.001$), and their respective bending angles, magnifications, time delays, and differential time delays. (a) The same as (a) of Table II. (b) The same as (b) of Table V. (c) The same as (a) of Table I.

β	Inner image on the same side as the source					Outer image on the same side as the source				
	θ_{is}	$\hat{\alpha}_{is}$	μ_{is}	τ_{is}	$\Delta\tau_{is}$	θ_{os}	$\hat{\alpha}_{os}$	μ_{os}	τ_{os}	
0.75	×	×	×	×	×	×	×	×	×	
0.85	0.985 460	0.270 920	-1.634 301	-577.4174	0.004 886	1.273 212	0.846 424	3.146 478	-577.4223	
2	0.632 970	-2.734 059	-0.038 933	-576.9387	0.841 932	2.488 924	0.977 849	1.150 355	-577.7807	
4	0.486 179	-7.027 642	-0.005 625	-573.9272	4.363 376	4.349 611	0.699 223	1.026 918	-578.2905	
6	0.415 912	-11.168 18	-0.001 874	-568.3368	10.325 23	6.262 637	0.525 273	1.008 728	-578.6620	
8	0.371 325	-15.257 35	-0.000 859	-560.2218	18.727 13	8.208 527	0.417 054	1.003 774	-578.9489	
10	0.339 464	-19.321 07	-0.000 467	-549.6044	29.577 00	10.172 36	0.344 712	1.001 941	-579.1814	
25	0.231 031	-49.537 94	-0.000 037	-390.9432	189.2497	25.074 04	0.148 084	1.000 121	-580.1930	
35	0.199 350	-69.601 30	-0.000 014	-208.0429	372.5350	35.053 54	0.107 070	1.000 043	-580.5779	
45	0.178 218	-89.643 56	-0.000 007	36.420 54	617.2886	45.041 91	0.083 823	1.000 020	-580.8680	

TABLE X. Magnification centroid due to lensing by the Schwarzschild black hole ($\nu = 1$); and weakly ($\nu = 0.7$), marginally strongly ($\nu = 0.5$), and strongly ($\nu = 0.04, 0.02, 0.001$) naked singularities. (a) The same as (a) of Table I.

β	Magnification centroid					
	$\nu = 1$ (SBH)	$\nu = 0.7$ (WNS)	$\nu = 0.5$ (MSNS)	$\nu = 0.04$ (SNS)	$\nu = 0.02$ (SNS)	$\nu = 0.001$ (SNS)
10^{-5}	0.000 015 000 000 000 4	0.000 015 000 000 000 3	0.000 015 000 000 000 3	0.000 014 999 999 343 3	0.000 014 999 989 507 3	×
10^{-3}	0.001 499 999 870 32	0.001 499 999 870 31	0.001 499 999 870 31	0.001 499 999 804 61	0.001 499 998 821 01	×
10^{-1}	0.149 870 601 362	0.149 870 601 362	0.149 870 601 361	0.149 870 594 833	0.149 870 497 099	×
2	2.490 707 198 63	2.490 707 198 62	2.490 707 198 62	2.490 707 176 80	2.490 706 848 78	2.428 167 682 65
4	4.388 236 394 45	4.388 236 394 45	4.388 236 394 45	4.388 236 390 45	4.388 236 321 68	4.328 563 385 84
6	6.290 110 811 74	6.290 110 811 74	6.290 110 811 74	6.290 110 810 57	6.290 110 780 80	6.251 795 026 25
8	8.227 195 245 92	8.227 195 245 92	8.227 195 245 92	8.227 195 245 33	8.227 195 222 97	8.201 829 221 37
10	10.185 550 248 9	10.185 550 248 9	10.185 550 248 9	10.185 550 248 4	10.185 550 228 0	10.167 771 538 0

TABLE XI. Magnification centroid shift due to lensing by the Schwarzschild black hole ($\nu = 1$); and weakly ($\nu = 0.7$), marginally strongly ($\nu = 0.5$), and strongly ($\nu = 0.04, 0.02, 0.001$) naked singularities. (a) The same as (a) of Table I.

β	Magnification centroid shift					
	$\nu = 1$ (SBH)	$\nu = 0.7$ (WNS)	$\nu = 0.5$ (MSNS)	$\nu = 0.04$ (SNS)	$\nu = 0.02$ (SNS)	$\nu = 0.001$ (SNS)
10^{-5}	$5.000 000 000 37 \times 10^{-6}$	$5.000 000 000 34 \times 10^{-6}$	$5.000 000 000 28 \times 10^{-6}$	$4.999 999 343 27 \times 10^{-6}$	$4.999 989 507 28 \times 10^{-6}$	×
10^{-3}	0.000 499 999 870 316	0.000 499 999 870 313	0.000 499 999 870 306	0.000 499 999 804 606	0.000 499 998 821 007	×
10^{-1}	0.049 870 601 361 8	0.049 870 601 361 5	0.049 870 601 360 9	0.049 870 594 832 6	0.049 870 497 098 7	×
2	0.490 707 198 627	0.490 707 198 624	0.490 707 198 620	0.490 707 176 798	0.490 706 848 782	0.428 167 682 651
4	0.388 236 394 450	0.388 236 394 449	0.388 236 394 447	0.388 236 390 447	0.388 236 321 681	0.328 563 385 839
6	0.290 110 811 742	0.290 110 811 742	0.290 110 811 741	0.290 110 810 567	0.290 110 780 796	0.251 795 026 246
8	0.227 195 245 922	0.227 195 245 922	0.227 195 245 921	0.227 195 245 327	0.227 195 222 966	0.201 829 221 370
10	0.185 550 248 860	0.185 550 248 859	0.185 550 248 859	0.185 550 248 432	0.185 550 228 011	0.167 771 538 043

TABLE XII. Total magnification due to lensing by the Schwarzschild black hole ($\nu = 1$); and weakly ($\nu = 0.7$), marginally strongly ($\nu = 0.5$), and strongly ($\nu = 0.04, 0.02, 0.001$) naked singularities. (a) The same as (a) of Table I.

β	Total magnification					
	$\nu = 1(\text{SBH})$	$\nu = 0.7(\text{WNS})$	$\nu = 0.5(\text{MSNS})$	$\nu = 0.04(\text{SNS})$	$\nu = 0.02(\text{SNS})$	$\nu = 0.001(\text{SNS})$
10^{-5}	138 816.932 541	138 816.932 541	138 816.932 542	138 816.941 647	138 817.077 259	×
10^{-3}	1388.169 595 52	1388.169 595 52	1388.169 595 53	1388.169 686 59	1388.171 042 70	×
10^{-1}	13.908 692 659 9	13.908 692 660 0	13.908 692 660 1	13.908 693 567 8	13.908 707 085 9	×
2	1.147 678 000 38	1.147 678 000 38	1.147 678 000 38	1.147 678 017 08	1.147 678 263 38	1.189 288 130 01
4	1.019 390 699 71	1.019 390 699 71	1.019 390 699 71	1.019 390 701 36	1.019 390 726 80	1.032 542 982 20
6	1.004 708 845 75	1.004 708 845 75	1.004 708 845 75	1.004 708 846 06	1.004 708 852 30	1.010 602 079 86
8	1.001 616 965 92	1.001 616 965 92	1.001 616 965 92	1.001 616 966 03	1.001 616 969 10	1.004 632 472 08
10	1.000 689 289 92	1.000 689 289 92	1.000 689 289 92	1.000 689 289 98	1.000 689 292 09	1.002 408 857 84

- [1] R. Penrose, in *Black Holes and Relativistic Stars*, edited by R. M. Wald (The University of Chicago Press, Chicago, 1998), p. 103.
- [2] R. M. Wald, arXiv:gr-qc/9710068.
- [3] K. S. Virbhadra, Phys. Rev. D **60**, 104041 (1999).
- [4] K. S. Virbhadra, D. Narasimha, and S. M. Chitre, Astron. Astrophys. **337**, 1 (1998).
- [5] K. S. Virbhadra and G. F. R. Ellis, Phys. Rev. D **62**, 084003 (2000). The light deflection in the vicinity of a photon sphere of a Schwarzschild black hole was also previously studied by some researchers; for example, C. Darwin, Proc. R. Soc. A **249**, 180 (1959); **263**, 39 (1961); H. C. Ohanian, Am. J. Phys. **55**, 428 (1987); R. J. Nemiroff, *ibid.* **61**, 619 (1993).
- [6] K. S. Virbhadra and G. F. R. Ellis, Phys. Rev. D **65**, 103004 (2002).
- [7] C.-M. Claudel, K. S. Virbhadra, and G. F. R. Ellis, J. Math. Phys. (N.Y.) **42**, 818 (2001).
- [8] V. Perlick, Living Rev. Relativity **7**, 9 (2004); Commun. Math. Phys. **220**, 403 (2001); Phys. Rev. D **69**, 064017 (2004); arXiv:0708.0178; W. Hasse and V. Perlick, Gen. Relativ. Gravit. **34**, 415 (2002).
- [9] A. F. Zakharov and Yu. V. Baryshev, Classical Quantum Gravity **19**, 1361 (2002); Int. J. Mod. Phys. D **11**, 1067 (2002); A. F. Zakharov, F. De Paolis, G. Ingrosso, and A. A. Nucita, New Astron. **10**, 479 (2005); Astron. Astrophys. **442**, 795 (2005).
- [10] P. Amore and S. Arceo Diaz, Phys. Rev. D **73**, 083004 (2006); P. Amore, S. Arceo, and F. M. Fernandez, *ibid.* **74**, 083004 (2006); P. Amore, M. Cervantes, A. De Pace, and F. M. Fernandez, *ibid.* **75**, 083005 (2007).
- [11] V. Bozza, S. Capozziello, G. Iovane, and G. Scarpetta, Gen. Relativ. Gravit. **33**, 1535 (2001); V. Bozza and L. Mancini, Astrophys. J. **627**, 790 (2005).
- [12] E. F. Eiroa, G. E. Romero, and D. F. Torres, Phys. Rev. D **66**, 024010 (2002); E. F. Eiroa and D. F. Torres, *ibid.* **69**, 063004 (2004); E. F. Eiroa, Braz. J. Phys. **35**, 1113 (2005); Phys. Rev. D **73**, 043002 (2006).
- [13] T. P. Kling, E. T. Newman, and A. Perez, Phys. Rev. D **61**, 104007 (2000); **62**, 024025 (2000); **62**, 109901(E) (2000); S. Frittelli, T. P. Kling, and E. T. Newman, *ibid.* **61**, 064021 (2000).
- [14] A. S. Majumdar and N. Mukherjee, Mod. Phys. Lett. A **20**, 2487 (2005); Int. J. Mod. Phys. D **14**, 1095 (2005); N. Mukherjee and A. S. Majumdar, Gen. Relativ. Gravit. **39**, 583 (2007).
- [15] C. R. Keeton and A. O. Petters, Phys. Rev. D **72**, 104006 (2005).
- [16] C. R. Keeton and A. O. Petters, Phys. Rev. D **73**, 044024 (2006); **73**, 104032 (2006); A. O. Petters, Mon. Not. R. Astron. Soc. **338**, 457 (2003); S. V. Iyer and A. O. Petters, Gen. Relativ. Gravit. **39**, 1563 (2007).
- [17] A. Bhadra, Phys. Rev. D **67**, 103009 (2003); R. Whisker, *ibid.* **71**, 064004 (2005); K. K. Nandi, *ibid.* **74**, 024020 (2006); G. N. Gyulchev and S. S. Yazadjiev, *ibid.* **75**, 023006 (2007); M. Safonova and D. F. Torres, Mod. Phys. Lett. A **17**, 1685 (2002).
- [18] S. Fernando and S. Roberts, Gen. Relativ. Gravit. **34**, 1221 (2002); C. Stornaiolo, Gen. Relativ. Gravit. **34**, 2089 (2002); K. Lake, Phys. Rev. D **65**, 087301 (2002); S. E. Vazquez and E. P. Esteban, Nuovo Cimento B **119**, 489 (2004); F. Finelli, M. Galaverni, and A. Gruppiso, Phys. Rev. D **75**, 043003 (2007).
- [19] M. P. Dabrowski and F. E. Schunck, Astrophys. J. **535**, 316 (2000); T. Matos and R. Becerril, Classical Quantum Gravity **18**, 2015 (2001); V. A. De Lorenci, N. Figueiredo, H. H. Fliche, and M. Novello, Astron. Astrophys. **369**, 690 (2001); F. E. Schunck, B. Fuchs, and E. W. Mielke, Mon. Not. R. Astron. Soc. **369**, 485 (2006); K. Sarkar and A. Bhadra, Classical Quantum Gravity **23**, 6101 (2006).
- [20] S. Wolfram, MATHEMATICA 6.0.
- [21] K. S. Virbhadra, Int. J. Mod. Phys. A **12**, 4831 (1997).
- [22] K. S. Virbhadra, S. Jhingan, and P. S. Joshi, Int. J. Mod. Phys. D **6**, 357 (1997).
- [23] P. Schneider, J. Ehlers, and E. E. Falco, *Gravitational Lenses* (Springer-Verlag, Berlin, 1992).
- [24] S. Weinberg, *Gravitation and Cosmology: Principles and Applications of the General Theory of Relativity* (Wiley, New York, 1972).
- [25] A. I. Janis, E. T. Newman, and J. Winicour, Phys. Rev. Lett. **20**, 878 (1968); M. Wyman, Phys. Rev. D **24**, 839 (1981); M. D. Roberts, Astrophys. Space Sci. **200**, 331 (1993).
- [26] F. Eisenhauer *et al.*, Astrophys. J. **628**, 246 (2005).
- [27] A. B. Congdon, C. R. Keeton, and C. E. Nordgren (unpublished).
- [28] R. R. Rafikov and D. Lai, Phys. Rev. D **73**, 063003 (2006).
- [29] K. P. Rauch and R. D. Blandford, Astrophys. J. **421**, 46 (1994).
- [30] M. C. Werner and A. O. Petters, Phys. Rev. D **76**, 064024 (2007).